Effect of grain size on structural transitions in anatase TiO_2: A Raman spectroscopy study at high pressure

G. R. Hearne,* J. Zhao, A. M. Dawe, V. Pischedda, M. Maaza, M. K. Nieuwoudt, P. Kibasomba, O. Nemraoui, and J. D. Comins
School of Physics, University of the Witwatersrand, Private Bag 3, Wits 2050, Johannesburg-Gauteng, South Africa

M. J. Witcomb
Electron Microscope Unit, University of the Witwatersrand, Private Bag 3, Wits 2050, Johannesburg-Gauteng, South Africa
(Received 23 June 2004; published 12 October 2004)

Micro-Raman spectroscopy has been used to investigate the structural stability of nanoanatase (TiO_2), of ~12 nm average grain size, up to pressures of ~40 GPa in a diamond anvil cell at room temperature. This has been compared to the Raman pressure behavior of bulk anatase, which undergoes a structural transition from the tetragonal structure to the orthorhombic α-PbO_2-type intermediate near ~5 GPa before transforming to the monoclinic baddeleyite structure at an onset pressure of ~15 GPa and remains in this phase up to the highest pressure of ~35 GPa. By contrast, the nanophase anatase maintains its structural integrity up to ~18 GPa before transforming directly to the baddeleyite structure, which is stable to the highest pressure of this study. The pressure dependence of the four most prominent Raman modes is similar for both the nanophase and bulk-anatase compounds suggesting that they have similar compressibilities, all of these modes exhibiting normal stiffening behavior as the pressure rises. In a separate temperature dependent micro-Raman study to 1000 °C at ambient pressure, the most intense (E_g) mode of both the nanophase and bulk-anatase samples shows unusual stiffening behavior on heating. This mode is associated with O-Ti-O bond-bending vibrations in which O displacements are bigger than the Ti displacements. In both samples, all other prominent Raman modes exhibit anticipated softening when heated. From these temperature and pressure dependences it may be deduced that intrinsic anharmonicity and associated phonon-phonon interactions govern the temperature dependence of the intense E_g mode, whereas either or both dilatation effects or intrinsic anharmonicity determine the behavior of the other modes. The linewidth of the most intense E_g mode in nanoanatase exhibits a sharp decrease from ambient to ~2 GPa, descending to a broad minimum at ~5 GPa, in contrast to the behavior of the bulk phase. The linewidth then increases monotonically at $P > 5$ GPa similar to the behavior of the bulk solid. This unusual behavior of the linewidth in the nanophase material may be explained by the effect of internal pressure acting across the curved surface in the nanosized grains being compensated by the externally applied pressure. The average grain size of ~12 nm of the nanoanatase is less than the critical size estimated for nucleation and growth of a new structural α-PbO_2-type phase. This rationalizes how the structural transition to the α-PbO_2-type intermediate phase, which occurs in bulk anatase, has been inhibited in the nanophase material. Instead, the formation of new grain boundaries of compacted nanoparticles of anatase would be the anticipated main pressure-induced structural modification, likely representing a lower free-energy situation than if nucleation of the new α-PbO_2-type intermediate with associated anatase/α-PbO_2-type interfaces occurred. At sufficiently high pressure the free-energy gain from the volume reduction to the baddeleyite phase is shown to offset the interface energy cost involved in the nucleation and growth of this high-pressure phase and, thus, drives the direct anatase→baddeleyite structural transition. Both the nanophase and bulk-sample pressure quench from the baddeleyite to the α-PbO_2-type structure upon decompression from 35–40 GPa to ambient conditions.

DOI: 10.1103/PhysRevB.70.134102 PACS number(s): 61.46.+w, 64.70.Kb, 78.30.−j, 81.40.Vw

I. INTRODUCTION

There has been considerable previous research to understand the pressure-induced structural transitions that occur in titanium dioxide (TiO_2).[1–10] Interest has been accelerated in recent years because the structural phases of TiO_2 and related compounds HfO_2 and ZrO_2 at high pressure exhibit a high bulk modulus. These structures obtained at high pressure may be retained upon decompression to ambient conditions and thus are prime candidates for ultrahard materials, these being important for a number of industrial applications.[7,11]

Three different structural phases of TiO_2 exist in nature, viz, anatase [Fig. 1(a)], rutile, and brookite. Other structures, such as the orthorhombic α-PbO_2-type phase [Fig. 1(b)] and the monoclinic baddeleyite phase [Fig. 1(c)], may be stabilized only under high pressure from a starting material of either anatase or rutile. A single crystal of anatase, for example, undergoes the following sequence of structural transitions under high pressure:

$$\text{anatase}(I4_1/amd) \rightarrow \alpha\text{-}PbO_2\text{-type phase}(Pbcn) \rightarrow \text{baddeleyite}(P2_1/c).$$

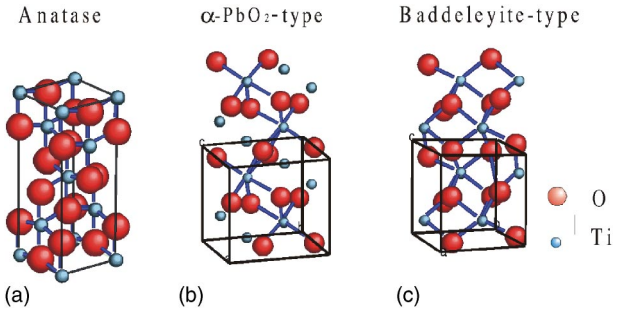

FIG. 1. Unit cells of different structural phases of TiO_2: (a) tetragonal anatase, (b) orthorhombic α-PbO_2-type phase, and (c) monoclinic baddeleyite phase.

The orthorhombic α-PbO_2-type phase is retained upon decompression to ambient conditions. Table I summarizes the main experimental results of high-pressure studies of anatase TiO_2. The differences in the transition pressures at which the structural transitions occur depend on whether the sample is single- or polycrystalline. Some of the most recent work of Arlt *et al.*[10] has shown that there may be a transition directly from the anatase to baddeleyite structure at ~13 GPa. They ascribed this to lattice defects and grain boundaries that suppress the transition of anatase to the α-PbO_2-type intermediate; however, no further details have been provided in their paper.

Nanostructured anatase TiO_2 has invoked considerable interest in recent years because it has a variety of potential applications, e.g., in photocatalysis and in photoelectrochemical solar cells.[12] The high surface-to-volume ratio in nano-particles affect the physical properties of the compound, e.g., temperature-induced microstructural evolution of nano-anatase TiO_2.[9,13–18] To the best of our knowledge there is only limited published work on the effect of the particle size of nanophase TiO_2 on the pressure-induced structural transitions,[19–21] in comparison to the wealth of research accomplished on the temperature-induced structural changes in this material.

Raman scattering is a convenient and sensitive probe widely used to characterize local structural changes and monitor structural transitions in compounds. The present work is primarily concerned with a micro-Raman investigation to ~40 GPa of nanoanatase TiO_2 of ~12 nm average grain size pressurized in a diamond anvil cell at room temperature.

II. EXPERIMENTAL

TiO_2 nanoparticles were synthesized by lyophilization. Titanium tetrachloride (99.99% Aldrich) starting salt was dissolved in distilled water to a desired concentration that determines the TiO_2 final-product particle size. Typically, 0.02 mol of dry anhydrous $TiCl_4$ was dissolved in 100 ml distilled water. The solution was flash frozen by injecting it at high pressure into liquid nitrogen through an ~80 μm nozzle with a central pin to break up the jet into a fine spray. The pulverized frozen mass was then transferred to the chamber of a Christ freeze-dryer operated at a pressure of 5 Pa where the drying operation commenced for ~24 hr. The lypohilized highly porous nanophase precursor salt was then decomposed by heating in air in the range of 300–700 °C for 3–30 min. The different structural phases of TiO_2 nanoparticles that may be stabilized (e.g., brookite, anatase, rutile) and the resultant average particle size are controlled mainly by the thermal decomposition temperature. Decomposition temperatures and the resultant structural phases that arise from the multicomponent precursor have been identified by thermal gravimetric analysis (TGA) and XRD investigations, respectively. Characterization of the nanoanatase sample was made by using both TEM as shown in Fig. 2 and by x-ray diffraction. The Scherrer formula has been used to deduce an average particle size of ~12 nm

TABLE I. Summary of the results of high-pressure studies of anatase TiO_2.

Phase transition	Anatase to α-PbO_2 type	α-PbO_2 type to baddeleyite	Anatase to baddeleyite	Method
Ohsaka *et al.* (Ref. 4)	2.6 GPa Polycrystalline			Raman spectroscopy
Haines and Leger (Ref. 7)	~7 GPa Polycrystalline	~10 GPa polycrystalline		x-ray diffraction
Lagarec and Desgreniers (Ref. 8)	4.5–7 GPa Single crystal	13–17 GPa polycrystalline		Raman spectroscopy
Arlt *et al.* (Ref. 10)	4.5 GPa Single crystal			Synchrotron x-ray diffraction
Arlt *et al.* (Ref. 10)			13 GPa Polycrystalline	Synchrotron x-ray diffraction
Swamy *et al.* (Ref. 19)			18GPa Nanophase (30–40 nm)	Synchrotron x-ray diffraction
This work			18 GPa Nanophase (~12 nm)	Raman spectroscopy
This work	5 GPa Bulk polycrystalline	12–15 GPa		Raman spectroscopy

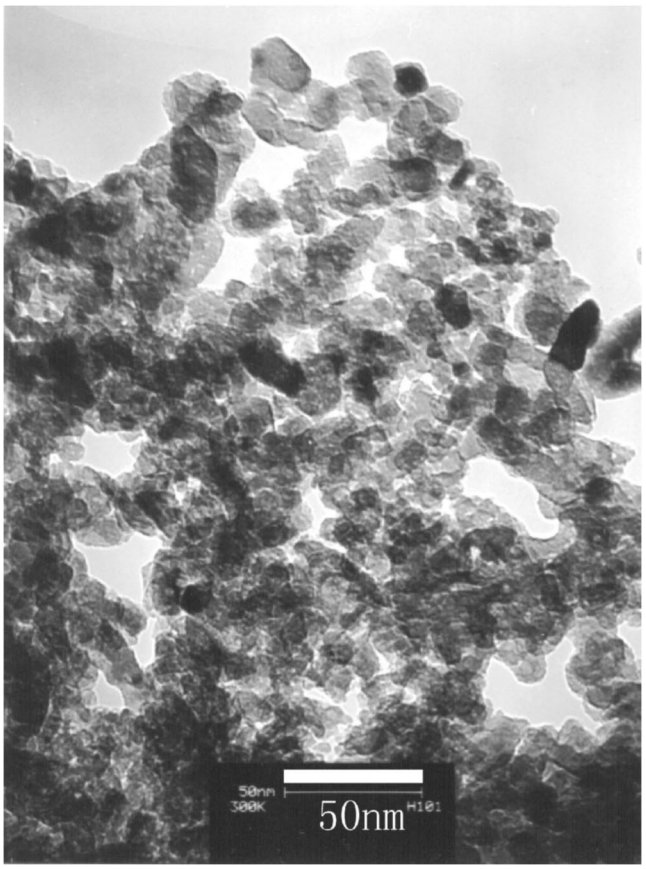

FIG. 2. Transmission electron micrograph (TEM) of as-received anatase TiO_2 nanoparticles.

from the (101) diffraction linewidth, consistent with the average value of the longest dimension of many of the irregular-shaped or platelet grains discerned in the TEM micrograph of Fig. 2. X-ray fluorescence measurements show that the sample is slightly off stoichiometry, namely, as $TiO_{1.92}$, which will give rise to some degree of Raman mode shifting and linewidth broadening[22] compared with the stoichiometric compound.

A piston-cylinder-type diamond anvil cell (DAC)[23] with anvil culets of 540 μm diam was used to generate high pressures up to ~38 GPa. After the T301 steel foil gasket had been pre-indented to ~40 μm from a starting thickness of ~250 μm, the sample was loaded into a cavity that had been spark eroded in the center of the preindentation. In one series of measurements, our new multiaperture gasket technique[24] was used to obtain Raman spectra in a single sequence of compressions of both nanophase and bulk crystalline anatase loaded into two separate cavities ($\phi \sim 100$ μm each) of the same preindented gasket. A second series of pressure measurements was performed on the nanophase sample alone. Liquid nitrogen was loaded into each sample cavity to serve as a pressure-transmitting medium by immersing the miniature DAC into a bath of the cryogen and momentarily releasing and then retightening the thrust-force screws.

Raman spectra in backscattering mode at room temperature and variable high pressures were obtained with a Jobin-Yvon T64000 spectrograph equipped with a Raman microscope, holographic gratings (1800 grooves mm^{-1}), and a liquid-nitrogen-cooled CCD detector. The 514.5 nm line of an Ar^+ laser with output power of 55 mW was used to excite the Raman scattering with the spectrograph operated in the triple-subtractive mode. Estimated laser power at the sample stage was 5 mW. The laser beam was focused onto the samples by means of an Olympus ×20 ultralong working distance objective, which results in a laser spot size of ~10 μm diam. The entrance-slit width of the premonochrometer was set at 200 μm. Under these conditions data acquisition times ranged from 30 s up to 600 s depending on the quality of the spectra. Pressure calibration within the cavity of the gasket was made in terms of the ruby *R*-luminescence lineshift[25] measured at the same position at which the Raman spectrum was obtained. The argon-ion laser plasma lines 516.3 nm, 516.6 nm, 517.6 nm, etc., were subsequently used for the Raman-shift calibration; these lines are removed from the Raman spectra presented in the figures of this paper.

III. RESULTS AND DISCUSSION

The pressure evolution of the Raman spectra of nanoanatase is shown in Figs. 3(a) and 3(b) whereas Raman spectra at a selected pressure of the bulk commercial sample are shown in Fig. 3(c). Under ambient conditions, the most prominent Raman bands in nanoanatase are at 146.4 cm^{-1} (E_g), 396.9 cm^{-1} (B_{1g}), 518.1 cm^{-1} (A_{1g}/B_{1g} unresolved doublet) and 641.3 cm^{-1} (E_g) where the band assignments have been indicated in brackets. These are part of six assigned Raman active modes ($A_{1g}+2B_{1g}+3E_g$) derived from factor group analysis[26] of tetragonal anatase, which belongs to the space group $D_{4h}^{19}(I4_1/amd)$. For bulk anatase the corresponding bands are at 141.3 cm^{-1}, 394.4 cm^{-1}, 516.1 cm^{-1} and 636.7 cm^{-1}. Part of the Raman peak-position shifts in the nanophase anatase may be due to deviations from stoichiometry known to affect both Raman line positions and widths.[22]

The pressure evolution of the Raman spectra of bulk anatase exhibits similar behavior to that reported in previous high-pressure studies.[8] As the pressure increases to ~5.6 GPa, several weak peaks appear at 331.0, 344.5, and 372.8 cm^{-1}, characteristic of the α-PbO_2-type phase. As pressure increases further, the intensities of these new peaks increase and they are clearly discerned at pressures of ~7.5 GPa and beyond, see Fig. 3(c). The structural transition of bulk polycrystalline anatase to the α-PbO_2-type intermediate was sluggish, as found previously,[7] coexisting with the original anatase structure up to ~15 GPa. Beyond this pressure, radically new Raman bands become apparent in the range of 225–280 cm^{-1} in addition to a prominent band at ~500 cm^{-1}; these are supposed to be characteristic of the high-pressure baddeleyite phase.[8]

The pressure evolution of the Raman spectra of the nanoanatase compound is quite different. No new peaks appear in the spectra up to ~16 GPa, which are all similar to the one at ambient pressure. Figures 3(a) and 4(a) show that the anatase phase in the nanostructured compound is stable to well beyond the transition pressure found in bulk anatase,

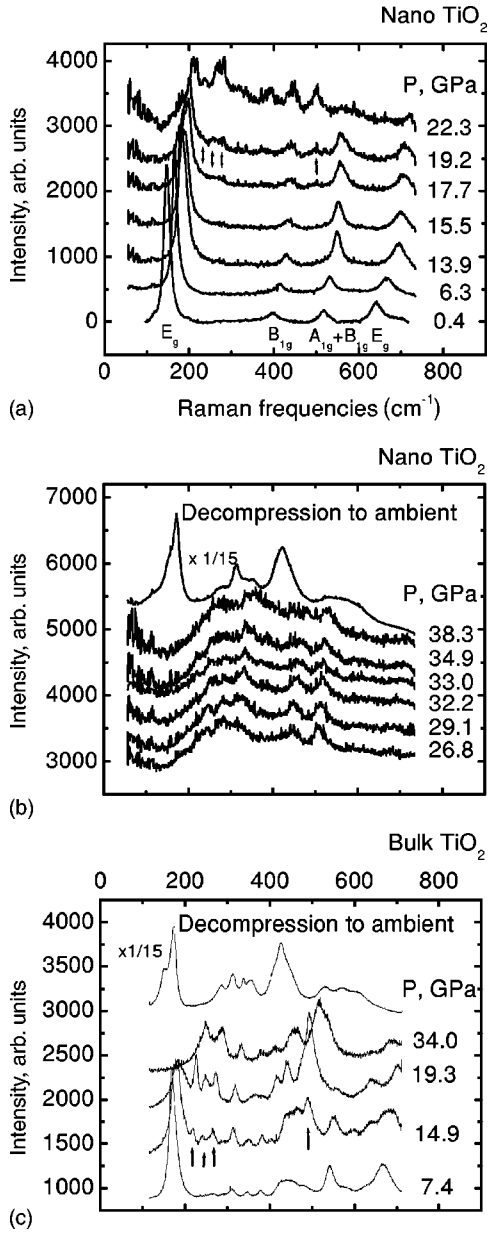

FIG. 3. Raman spectra under high pressure of nanostructured anatase (a), (b); Panel (c) is for bulk anatase. The arrows in panels (a) and (c) are to delineate new modes specific to the baddeleyite phase.

i.e., ~5 GPa. When the pressure is increased to 17.7 GPa, see Fig. 3(a), a number of new bands of low intensity are discerned at ~235 cm^{-1}, ~250 cm^{-1}, ~275 cm^{-1}, and ~500 cm^{-1}, which appear to be specific to the high-pressure baddeleyite phase[8] and which persist to the maximum applied pressure of ~38 GPa. Although, the spectra at the higher pressures, $P > 26$ GPa, have much broader bands than in the bulk sample. This may arise from one, or a combination, of the following factors: imminent pressure-induced amorphization as seen previously,[21] the effect of nonhydrostatic stress at these elevated pressures, possible changes to the morphology of the nanoparticles, fracturing of the nanoparticles to smaller subunits.

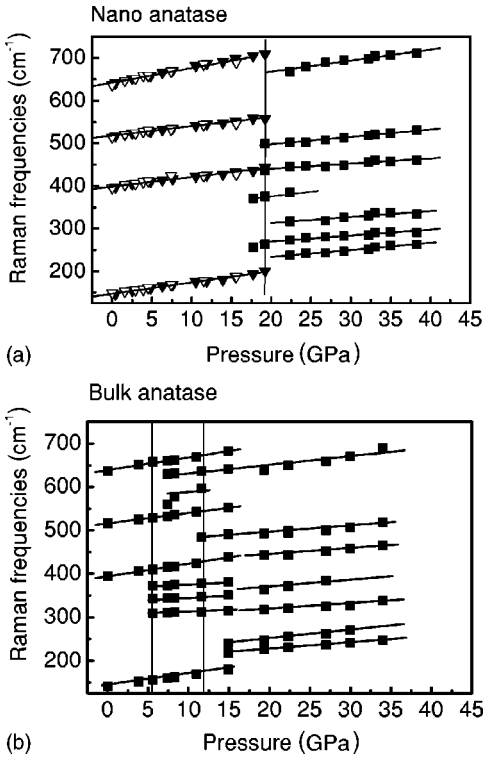

FIG. 4. Pressure dependence of frequencies of Raman active modes of (a) nanoanatase compared with that of bulk anatase in (b). Thin vertical lines show the onset pressures of structural transitions.

These results clearly demonstrate that the nanophase sample transforms directly from the anatase to baddeleyite structure at 17.7 GPa without passage via the α-PbO_2-type intermediate, consistent with a previous pressure study on nanoanatase.[21] However, when the nanophase sample is decompressed from the maximum pressure, the high-pressure baddeleyite phase is quenched to the α-PbO_2-type phase, similar to the behavior of the bulk compound [see Figs. 3(b) and 3(c)], albeit with broader Raman bands.

Raman mode frequencies of the nanophase sample as a function of pressure are shown in Fig. 4(a). The pressure dependence of the Raman frequencies ($d\nu/dP$) have been obtained by linear fits [solid curves in Fig. 4(a)] over the pressure range before and after the structural transition that occurs at ~18 GPa. The hollow and filled symbols simply delineate measurements from the two different series of measurements. The slope $d\nu/dP$ averaged over the most intense bands of nanophase anatase is 2.58 ± 0.22 cm^{-1} GPa^{-1} compared with bulk anatase in Fig. 4(b) where the slope $d\nu/dP$ average is 2.70 ± 0.13 cm^{-1} GPa^{-1}, perhaps indicating that the anatase phase in both compounds have similar compressibilities.

After the transition of nanophase anatase to the baddeleyite structure, the average $d\nu/dP$ of the high-pressure phase is 1.65 ± 0.21 cm^{-1} GPa^{-1}, suggesting that the baddeleyite phase is less compressible than the low-pressure anatase phase. This is qualitatively consistent with the compressibilities derived from the recent x-ray diffraction measurements.[10]

Figure 5(a) shows the pressure-induced changes of the linewidth of the intense E_g band of the bulk anatase com-

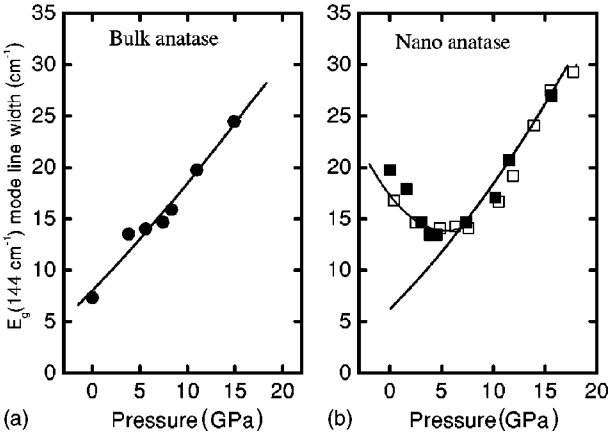

FIG. 5. Pressure dependence of the line width of the intense E_g Raman active mode (at ~144 cm^{-1} under ambient conditions) of anatase TiO_2: (a) for the bulk solid and (b) for the nanostructured material. Thin solid lines are to guide the eye.

pound; the linewidth increases from 7 cm^{-1} at ambient pressure to 25 cm^{-1} at ~15 GPa. There is an inflection at ~5 GPa perhaps attributable to the volume reduction that occurs when anatase transforms to the α-PbO_2-type phase.[7,10]

The linewidth of the intense E_g mode of nanophase anatase, by contrast, displays very different pressure behavior as shown in Fig. 5(b). The linewidth first decreases rapidly up to 1.5 GPa, reaching a broad minimum that extends up to ~5 GPa, followed by an upturn and monotonic increase as the pressure rises beyond 5 GPa. The pressure at which the broad minimum shows an upturn is close to the transition pressure of ~5 GPa where bulk anatase transforms to the α-PbO_2-type structure.

The intense E_g band (located at ~144 cm^{-1} under ambient conditions) of anatase, which arises from O-Ti-O bond-bending-type vibrations of the structure[4] has a linewidth or line shape affected by various factors. These include nonstoichiometry due to oxygen deficiencies or disorders induced by minority phases.[22,27] In addition, linewidth broadening in nanodimensioned particles may arise from the pressure effect induced by the surrounding particles or the surface stress of the particle.[28] Phonon confinement effects in nanoparticles also affect the line shape, and several authors have discussed the relation between increasing linewidth of the intense E_g mode at ~144 cm^{-1} with particle-size reduction in nanophase anatase using this idea.[15,18,29,30] In this case the correlation between the E_g linewidth and particle size has been corroborated by measurements of particle size deduced from x-ray diffraction and TEM.

To understand the unusual behavior of the E_g mode linewidth in nanophase anatase, additional Raman and XRD pressure measurements have been made up to 6.2 GPa followed by measurements upon decompression to ambient conditions. The Raman investigation shows that the change of linewidth with pressure is reversible upon pressure cycling from ambient up to 6.2 GPa and back to ambient pressure again, as shown in Fig. 6(a). The linewidth of the original as-received sample is 22.2(2) cm^{-1} compared to that of the decompressed sample, 23.8(4) cm^{-1} at ambient pressure.

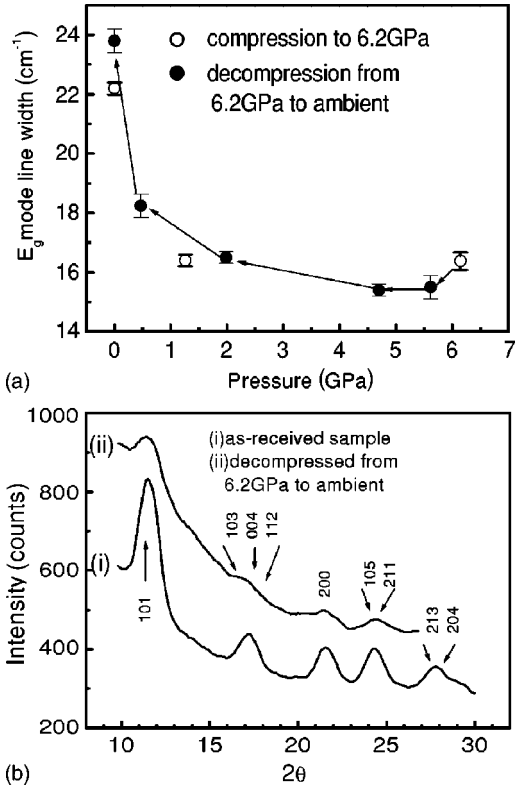

FIG. 6. (a) Detailed cyclic-pressure behavior of the intense E_g mode linewidth up to ~6 GPa. (b) XRD patterns prior and subsequent to pressure cycling.

The x-ray diffraction pattern of the sample after decompression from 6.2 GPa to ambient pressure as shown in Fig. 6(b) was obtained by using a Siemens SMART diffractometer with CCD area detector. The intensities of the x-ray pattern of the decompressed sample are weaker and broadened, but the diffraction peak positions do not show obvious differences when compared to that of the as-received sample. If the background contribution in both x-ray diffraction patterns are eliminated in Fig. 6(b), the half-width at half maximum (HWHM) of the (101) diffraction peak are 1.44(6)° for the as-received sample and 1.81(8)° for the decompressed sample. Therefore, the increase in linewidths of both the E_g Raman mode and (101) Bragg reflection after decompression to ambient pressure perhaps rules out the possibility of pressure-induced grain growth (coarsening) when the sample is pressurized to ~6 GPa. Such a grain-coarsening mechanism is expected to be irreversible and any consequent linewidth narrowing of diffraction peaks that occur should persist when the sample is decompressed to ambient conditions.

For small near-spherical particles embedded in a host matrix, viz, nanophase anatase in a nitrogen pressure-transmitting medium, we may consider the contents of the TiO_2 nanoparticle to experience an extra pressure ΔP resulting in the curvature of the nanoanatase/nitrogen interface, just as the contents of a liquid drop involve an extra pressure ΔP.

If P_i and P_e are the pressures at the interior and exterior of the nanoparticle, respectively, then the excess pressure $\Delta P = P_i - P_e$ across a curved or any planar surface is

$$\Delta P \propto f/d, \tag{1}$$

where f is the surface stress and d the linear dimension of the particle.[31,32]

The concept of surface stress f is applicable to a solid surface and is related to the surface-free energy σ, which constitutes a significant part of the total free energy of nanodimensional particles. The surface-free energy is defined as the reversible work per unit area or force per unit length of exposed edge involved in forming *new* surface material. In the case of a liquid where surface shear stresses and associated elastic strains along the surface cannot be sustained, the surface-free energy is referred to as the surface tension. However, in solid surfaces the surface area may be changed by deforming the surface *elastically*, keeping the number of surface lattice sites constant. In this case the work per unit area or force per unit length of exposed edge to change the surface area is not equal to the surface-free energy and is instead referred to as the surface stress f. If the work necessary to deform area A by increasing it by dA in the isotropic case is considered, then surface stress f is related to the surface free energy σ by[28,33]

$$f = \sigma + A\frac{d\sigma}{dA}. \tag{2}$$

In a bulk grain this extra pressure ΔP of Eq. (1) is considered to be negligible because of the dependence on the inverse linear dimensions of the grain.

Diffraction patterns at ambient conditions, with 2θ ranging from 10° to 80°, were measured on a Siemens capillary diffractometer. Data were refined using the standard analyzing programs WINCELL[34] or GSAS[35] to obtain the lattice parameters. Measurements of the lattice parameter of the NIST Si640C standard on this instrument indicated that there was a systematic error of ±0.02%, hence, lattice parameters cannot be determined to a higher precision than this. At ambient pressure the lattice parameter of the nanoanatase was found to be $a_o = 3.776 \pm 0.008$ Å and $c_o = 9.50 \pm 0.02$ Å ($V_0 = 135.5 \pm 0.7$ Å^3) and compared to the bulk sample for which $a_o = 3.785 \pm 0.002$ Å and $c_o = 9.513 \pm 0.004$ Å $V_0 = 136.3 \pm 0.4$ Å^3. This may be compared with the standard data $a_0 = 3.785$ Å and $c_0 = 9.513$ Å of bulk anatase.[36] These measurements suggest that there is possibly a slight reduction in the unit-cell volume of the nanophase material, as expected for a nanoparticle that is likely to experience an excess internal pressure across a curved boundary, as quantified in Eq. (1).

In the case of spherical particle of diameter d, the excess pressure from Eq. (1) may be written as involving surface stress

$$\Delta P = \frac{4f}{d}. \tag{3}$$

In a first approximation we equate surface tension and surface stress $\gamma = f$, although it should be recognized that f may be up to 3 times greater than this.[37,38] Using the accepted value[32] of $\gamma \sim 1.5$ Jm^{-2} we obtain from Eq. (3) an excess pressure of $\Delta P = 0.5$ GPa. The excess pressure in 12 nm diam spherical particles is then likely to be as high as $\Delta P \sim 1.5$ GPa, if it is taken into account that surface stress $f > \gamma$ should be used in Eq. (3).

Figure 5(a) shows that the linewidth of the intense E_g mode increases for a grain that is under pressure. At ambient pressure, part of the line broadening in the Raman spectrum of the nanoparticle of anatase is supposed to arise from the extra internal pressure that causes the curvature of the surface. Note also the strong pressure dependence of the linewidth up to $P \sim 1.5$ GPa in the nanophase material. As this sample is pressurized in the cavity of the gasket, the external pressure P_e rises and there is a corresponding decrease in the net pressure ΔP acting on the contents of each nanoparticle. Thus as external pressure P_e rises to compensate the internal pressure P_i, the net pressure ΔP on the nanoparticle diminishes and an associated decrease in the linewidth is expected. This proffers an explanation for the pressure dependence of the linewidth [see Fig. 6(a)] as external applied pressure rises and compensates the excess pressure ΔP internal to the particle. There is no net pressure on the contents of the nanoparticle at ~1.5 GPa, where the rapid pressure dependence of the linewidth changes drastically and the linewidth is almost at its minimum value. Any line broadening at this point is due to any one, or a combination, of the mechanisms mentioned previously, e.g., phonon confinement effects. As the applied pressure rises beyond ~1.5 GPa, the nanoparticle is then subjected to an increasing net pressure, $P_e > P_i$, from the externally applied stresses transmitted through the nitrogen medium, similar to the case of bulk anatase in Fig. 5(a). From the linewidth behavior in Figs. 5(b) and 6(a) we infer that the excess pressure in the nanoparticles is in the range of 1.5 to 5 GPa at ambient external pressure. The broad minimum may be a result of a number of factors, including a distribution of particle dimensions, some of the nanoparticles perhaps being nonspherical platelets,[39] and compaction of the grains with some consequent effect on grain boundaries or surfaces (i.e., on the f values). The broad minimum is thus supposed to represent the range of pressures required to counterbalance a range of internal pressures across a range of surface dimensions and surface stresses. Alternatively, the broad minimum may be due to fracturing of the nanoparticles to smaller subunits (with a distribution of sizes), as a result of the applied quasihydrostatic stresses in the sample cavity, and there is, consequently, an increase in excess pressure according to Eq. (1).

The behavior of the E_g-mode linewidth in the range ambient to 5 GPa is almost reversible when the external pressure is reduced to zero, [see Fig. 6(a)], albeit perhaps slightly broader in the decompression cycle. This implies that the net pressure on the particle reverts back to or in excess of ~1.5 GPa due to internal pressure P_i, which is consistent with the elastic deformation model we have proposed where a net pressure ΔP is responsible for part of the line broadening.

In situ Raman studies were also performed as a function of temperature to 1000 °C on both the nanophase and bulk anatase compounds. The temperature dependence of the Raman modes is presented here to emphasize the different effects of pressure and temperature on the modes, in particular the intense E_g mode at ~144 cm^{-1}. The Raman measurements at elevated temperatures were performed by using a

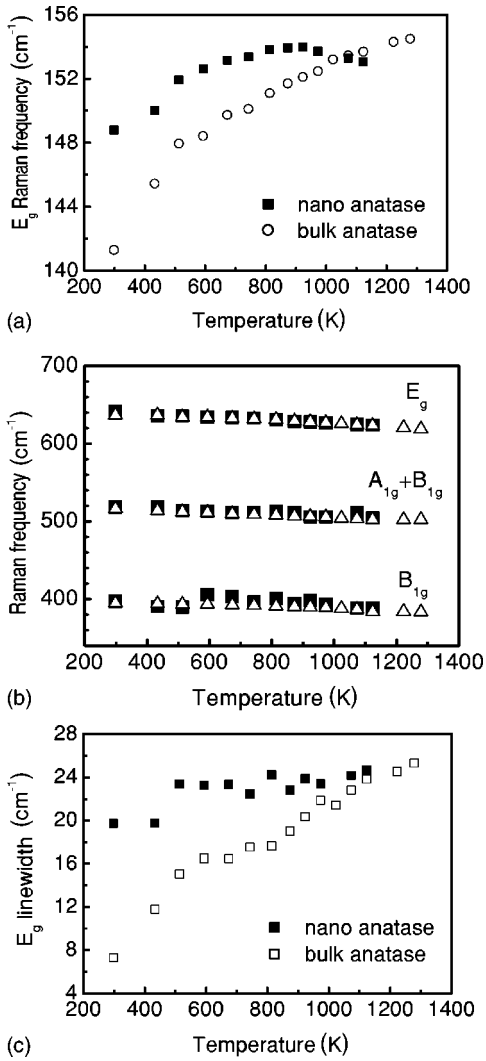

FIG. 7. (a) Temperature dependence of the intense E_g Raman mode frequencies of both nano- and bulk anatase. (b) Temperature dependence of the other Raman active mode frequencies of both nano- and bulk-anatase, solid and hollow symbols, respectively. (c) Temperature dependence of the linewidth of the intense E_g mode.

Linkham T600 high-temperature stage with the sample in an argon gas atmosphere. After the samples are stabilized at a new temperature with a drift not exceeding ±1 °C, a Raman spectrum has been collected first from the nanophase sample in a typical acquisition time of 720 s and then the much more intense spectrum from the bulk sample is collected in 7 s. This ensures that both samples have been heated for a comparable amount of time.

Figure 7(c) shows the change of the Raman linewidth of the intense E_g mode of the bulk solid is close to linear as temperature rises above 160 °C. Whereas in the nanostructured sample, the linewidth of this mode appears to be nearly constant above this temperature. In the bulk compound the linear increase in intense E_g mode linewidth is typically due to thermal expansion effects and an increasing atomic mean-square-displacement (msd), analogous to the effect of increasing disorder as the temperature rises. In the nanostructured compound, the effect of increasing temperature is similar to sintering and associated grain-coarsening effects. We suppose that both phonon confinement in nanodimensioned anatase as well as internal pressure are partly responsible for the excess linewidth of the intense E_g mode at ambient external pressure, as depicted in Fig. 5. Grain growth at high temperatures will decrease both these effects as the dimensions of each grain increases and we may expect a corresponding decrease in the linewidth. This will be counteracted by concurrent thermal effects of lattice expansion and an increased msd or thermally induced disorder leading to linewidth broadening. As a consequence of these two competing effects we may expect the linewidth to remain nearly constant.

An interesting feature of the intense E_g mode at $\sim 144\ \mathrm{cm}^{-1}$ is that it exhibits hardening as the temperature rises, whereas typical softening and an associated decrease in frequency is expected as seen in the behavior of the other modes of the anatase phase, see Figs. 7(a) and 7(b).

By considering each vibrational mode ν to be a function of volume V and temperature T, the temperature dependence $d\nu/dT$ at constant pressure may be expressed as

$$\left(\frac{\partial \ln \nu}{\partial T}\right)_P = -\left(\frac{\beta}{\kappa}\right)\left(\frac{\partial \ln \nu}{\partial P}\right)_T + \left(\frac{\partial \ln \nu}{\partial T}\right)_V. \tag{4}$$

This involves similar notation to that of Peercy and Morosin[40] and Samara and Peercy,[2] where $\beta=(\partial \ln V/\partial T)_P$ is the volume thermal-expansion coefficient and $\kappa=-(\partial \ln V/\partial P)_T$ is the compressibility defined previously. This equation may be rewritten in terms of the measured pressure and temperature dependences of the Raman-active mode, viz, as

$$(\Delta \nu_T)_P = -(\Delta \nu_P)_T + (\Delta \nu_T)_V, \tag{5}$$

where the left-hand side is the *measured* change (temperature dependence) of ν on raising the temperature from 0 to T K at constant pressure of 0.01 MPa (1 bar). The first term on the right-hand side is the change in ν caused by raising the pressure—at constant temperature T—to a value P sufficient to cause the same volume change as the term on the left-hand side of (4). In accord with Eq. (4) this term may be obtained from β and the mode Gruneisen parameter

$$\gamma = \frac{1}{\kappa}\left(\frac{1\partial \nu}{\nu \partial P}\right)_T,$$

which involves the *measured* pressure dependence of the mode. The second term on the right-hand side of Eq. (5) is the change in ν by raising the temperature from 0 to T K at constant volume (i.e., volume of the crystal at 0 K).

Thus Eqs. (4) and (5) serve to emphasize that the frequency shift at constant pressure has a pure volume contribution and a pure temperature contribution. Both of these contributions find their origin in the anharmonicity of the interatomic potentials, i.e., deviation from harmonic quadratic behavior. The frequency shift Δ of a particular phonon mode due to anharmonicity, to lowest order in perturbation theory, may be denoted

TABLE II. Logarithmic temperature and pressure derivatives at room temperature for the Raman modes of both nano and bulk anatase phase. These have been used to calculate the intrinsic anharmonicity $(\partial \ln \nu/\partial \mathrm{T})_{\mathrm{V}}$ from Eq. (4).

Bulk anatase	E_g (141.3 cm^{-1})	B_{1g} (394.4 cm^{-1})	$A_{1g}+B_{1g}$ (516.1 cm^{-1})	E_g (636.7 cm^{-1})
$(\partial \ln \nu/\partial \mathrm{T})_{\mathrm{P}}$ (10^{-5} K^{-1})	12.49±0.07	−5.5±0.1	−2.9±0.1	−3.2±0.1
$(\partial \ln \nu/\partial \mathrm{P})_{\mathrm{T}}$ (10^{-3} GPa^{-1})	15.8±0.5	7.0±0.2	4.5±0.1	4.4±0.3
$\beta \times B \times (\partial \ln \nu/\partial \mathrm{P})_{\mathrm{T}}$ (10^{-5} K^{-1})	7.7±0.5	3.4±0.2	2.2±0.1	2.2±0.2
$(\partial \ln \nu/\partial \mathrm{T})_{\mathrm{V}}$ (10^{-5} K^{-1})	20.2±0.6	−2.1±0.3	−0.7±0.2	−1.0±0.3
Bulk anatase	E_g (146.4 cm^{-1})	B_{1g} (396.9 cm^{-1})	$A_{1g}+B_{1g}$ (518.1 cm^{-1})	E_g (641.3 cm^{-1})
$(\partial \ln \nu/\partial \mathrm{T})_{\mathrm{P}}$ (10^{-5} K^{-1})	11.84±0.07	−5.1±0.2	−2.8±0.2	−3.0±0.1
$(\partial \ln \nu/\partial \mathrm{P})_{\mathrm{T}}$ (10^{-3} GPa^{-1})	15.3±0.6	5.3±0.2	4.1±0.1	5.3±0.5
$\beta \times B \times (\partial \ln \nu/\partial \mathrm{P})_{\mathrm{T}}$ (10^{-5} K^{-1})	7.5±0.5	2.6±0.2	2.0±0.1	2.6±0.2
$(\partial \ln \nu/\partial \mathrm{T})_{\mathrm{V}}$ (10^{-5} K^{-1})	19.3±0.6	−2.5±0.4	−0.8±0.3	−0.4±0.3

$$\Delta = \Delta^E + (\Delta^3 + \Delta^4) \equiv \Delta^E + \Delta^A, \tag{6}$$

where Δ^{E} represents the renormalized frequencies of independent harmonic oscillators in the dilatated lattice as a result of the volume change $\Delta V/V$ from thermal expansion, and this is commonly referred to as a quasiharmonic contribution. In most solids $\Delta^{\mathrm{E}}<0$, i.e., the dilatation results in softening. The frequency shifts Δ^3 and Δ^4 arise from *phonon-phonon* interactions and are from the lowest-order effects of cubic and quartic terms of the interatomic potential (see Kolk[41] pp. 75–78). The multiphonon process associated with the cubic term of the interatomic potential gives rise to a negative frequency shift Δ^3, whereas the shift Δ^4 associated with quartic anharmonicity is positive.[42] Therefore, the resultant frequency shift due to phonon-phonon interactions Δ^{A} may be either positive or negative depending on the relative magnitudes of the anharmonic terms in the interatomic potential.

Comparing Eqs. (4) or (5) to Eq. (6) it may be noted that the first term on the right-hand side of the equations is derived from quasiharmonic effect, i.e., frequency shift due to the volume change $-(\Delta \nu_P)_T = \Delta^{\mathrm{E}}$. The second term on the right-hand side is from the intrinsic anharmonicity and associated effect of higher-order terms rather than from the quadratic of the interatomic potential, hence $(\Delta \nu_T)_V = \Delta^{\mathrm{A}}$.

The temperature dependences of the phonon modes depicted in Fig. 7 may now be rationalized in terms of the pressure dependences of Fig. 4 and using Eqs. (4)–(6). The pressure dependence for each prominent anatase mode is positive $(\partial \nu/\partial P)_T > 0$ and, therefore, as part of the first term in Eq. (4) contributes a negative softening behavior to the overall temperature dependence of each mode $-(\Delta \nu_P)_T = \Delta^{\mathrm{E}} < 0$. Figure 7 indicates that $(\partial \nu/\partial T)_P > 0$ for the E_g mode, and this hardening must then originate from the phonon-phonon interactions that contribute positive frequency shifts $\Delta^{\mathrm{A}} > 0$ (e.g., likely quartic anharmonicity effects) that dominate the quasiharmonic effect $|\Delta^{\mathrm{A}}| > |\Delta^{\mathrm{E}}|$. For all the other modes, the converse may be true $|\Delta^{\mathrm{A}}| < |\Delta^{\mathrm{E}}|$, and the softening occurs mainly because of the dilatation, alternatively, phonon-phonon interactions are such that softening (e.g., dominant cubic anharmonicity) occurs, $\Delta^{\mathrm{A}} < 0$.

Quantitative estimates of the intrinsic anharmonicity, $(\partial \ln \nu/\partial \mathrm{T})_{\mathrm{V}}$, for each prominent anatase mode is obtained from the measured pressure and temperature dependences $(\partial \ln \nu/\partial \mathrm{P})_{\mathrm{T}}$ and $(\partial \ln \nu/\partial \mathrm{T})_{\mathrm{P}}$ at room temperature as obtained from linear fits to the data in Figs. 4 and 7, respectively, and by using Eq. (4). These values have been listed in Table II and may be compared with the case of rutile-type SnO_2 measured by Peercy and Morosin[40] or rutile-type TiO_2 by Samara and Peercy.[2] For the calculations in Table II, $B = 1/\kappa = 180$ GPa (Ref. 10) and $\beta = (\partial \ln V/\partial \mathrm{T})_{\mathrm{P}} = 27.2 \times 10^{-6}$ K^{-1} at room temperature[43] have been used. It appears that the intense E_g mode, corresponding to O-Ti-O bond-bending vibrations in which the oxygen atoms undergo larger displacements than the titanium,[26] exhibits pronounced intrinsic anharmonicity compared to the other prominent modes. There is some degree of intrinsic anharmonicity in the B_{1g} mode at ~395 cm^{-1}, also corresponding to O-Ti-O bond bending, but with the titanium ion displacements being larger than that of the oxygens. Whereas the other prominent modes exceeding 500 cm^{-1}, arising from Ti-O bond-stretching-type vibrations, have appreciably less intrinsic an-

harmonicity. This perhaps provides some insight into which optical modes in the anatase structure are linked to physical properties of the compound, which are determined by anharmonic interatomic potentials, e.g., thermal expansion behavior.

We now attempt to explain why the nanostructured material transforms directly to the baddeyelite structure and why this occurs at a higher value of applied pressure compared to the behavior of the bulk compound. As the TEM micrograph shows in Fig. 2, the as-received sample consists of nanodimensional grains that often aggregate by means of the Van der Waals interaction. When the sample is pressurized the density of the sample is supposed to increase when loose grains pack together and, consequently, new interfaces or grain boundaries form.

In considering the nucleation of a new phase, e.g., spherical nuclei of the α-PbO_2-type intermediate, the minimum or critical diameter d^* for self-sustaining growth of the nucleus and the nucleation energy barrier ΔG^* in the case of homogeneous nucleation is given by[31]

$$d^* = \frac{4\gamma}{\Delta G_V - \Delta G_S}, \tag{7}$$

and

$$\Delta G^* = \frac{16\pi\gamma^3}{3(\Delta G_V - \Delta G_S)^2}. \tag{8}$$

Both equations are seen to be dependent on the interfacial energy γ that exists between interfaces of the new phase and the host matrix. ΔG_V is the free-energy reduction per unit volume due to the increase in density at the structural transition and ΔG_S is the misfit strain energy per unit volume. The two equations above are derived from minimizing the total free-energy change including the free-energy increase $A\times\gamma$ from the creation of new surface area A in the nucleation process.

To estimate d^* from Eq. (7), we use the accepted value for the surface stress value, i.e., $\gamma = f \approx 1.5$ Nm^{-1}. The reduction in free energy per unit volume due to density increase $\Delta G_V = P(\Delta V/V)$ is estimated by assuming that the structural transition would occur at $P \sim 5$ GPa and that the relative change in the unit-cell volume $\Delta V/V$ of ~ 10 %, being similar to bulk values.[10] The estimated critical diameter is then $d^* \sim 15$ nm, for the case where the misfit strain-energy contribution has been neglected in Eq. (8). If it was to be included, then the critical diameter may be slightly larger.[31,44] It may be noted that the expression for the critical diameter (dimensions) [Eq. (7)] is true also for the case of heterogeneous nucleation, e.g., at grain boundaries where d^* is some linear dimension of the nucleus that is not necessarily spherical.[31] Also, in the case of heterogeneous nucleation, Eq. (8) would be multiplied by a shape factor $S(\theta)$, which is smaller than unity,[31] implying that shape deviation from spherical helps to lower the nucleation energy barrier ΔG^* in a heterogeneous system.

Therefore, the above estimates indicate that the α-PbO_2-type intermediate will only nucleate and grow as a stable particle if it has a diameter $d > 15$ nm, else it constitutes a cluster or embryo and collapses. Since the nanophase anatase particles have average dimensions of $d \sim 12$ nm, they are therefore smaller than d^* and may be considered to be embryonic. In the case of a nanoparticle of anatase of diameter $d < d^*$ it costs too much free energy, of order $\gamma \times d^2$, to transform to a new structural phase with α-PbO_2 surfaces of dimension d^2.

This suggests that lower-energy grain boundaries occur in the compacted nanoparticles of anatase, apparently energetically more favorable than the formation of anatase/α-PbO_2-type interfaces. Consequently, compacted nanophase anatase persists to high pressures in preference to the nucleation of a metastable α-PbO_2-type intermediate that occurs in the bulk solid. From Eq. (7) we again estimate the critical diameter for nucleation and growth of the baddeleyite phase at ~ 15 GPa using the relative volume reduction $\Delta V/V \sim 15$ % at the anatase $\rightarrow$ baddeleyite transition, typical of what has been measured in a bulk single-crystal.[10] A value for this critical diameter $d^* \sim 4$ nm is obtained if $\gamma \sim 1.5$ Nm^{-1} is used, which is similar to the value of surface stress f value used for nanoanatase and if the misfit strain energy ΔG_S is neglected. This demonstrates that the critical diameter d^* is appreciably smaller than the dimensions of the anatase nanoparticles. So nucleation and growth of the new baddeleyite phase out of the original anatase nanoparticle is plausible, consistent with the experiment observations. At sufficiently high pressures, the free-energy decrease $\Delta G_V \sim P(\Delta V/V)$ due to the density increase at the anatase $\rightarrow$ baddeleyite transition is sufficient to counterbalance the increase in surface energy $\gamma \times d^2$ of the particles of the new phase that nucleate at the transition, so that nucleation and growth of the new baddeleyite phase is energetically favored. It may be noted that even though nanophase anatase does not transform to the α-PbO_2-type intermediate upon compression to the maximum pressure of this study at 35–40 GPa, the high-pressure (nanophase) baddeleyite phase back transforms to the α-PbO_2-type structure and not to the original anatase structure upon pressure release to ambient conditions. The bulk high-pressure phase behaves in a similar way under decompression.

Nanophase anatase appears to transform directly to the baddeleyite structure at an externally applied pressure of 17–18 GPa according to the Raman data of Figs. 3 and 4; note that this is higher than the transition pressure of the bulk material. One possible explanation for this is that the internal pressure distribution P_i is in the range of 1–3 GPa due to either (or both) particle-size and surface-stress distributions in the absence of external applied stresses, as inferred from the linewidth data of Fig. 5. Then at an applied pressure of ~ 18 GPa, there is a net pressure in the range of $|\Delta P| \sim 15$–17 GPa on the distribution of nanoparticles. It is in this range that values of the externally applied pressure in the bulk compound (for which P_i is negligible) induce a transformation to the baddeleyite structure from a low-pressure precursor.

A potentially interesting subject of future pressure studies of nanostructured anatase is to check whether there are indeed critical grain sizes $d \sim 12$ nm below which compacted anatase would exhibit the formation of lower-energy grain

boundaries in preference to nucleation of new surfaces of the α-PbO_2-type intermediate, whereas at $d > 12$ nm the α-PbO_2-type intermediate does nucleate and grow. This may also be a general feature of nanostructured systems, indicating that the passage to new structural states so as to minimize free energies when P or T is changed may be quite different from the bulk.

ACKNOWLEDGMENTS

Funding for this project has been derived from the NRF-Pretoria. The assistance of our Structural Chemistry Group in the School of Chemistry and the Council for Geosciences (Pretoria-Tshwane) in obtaining some of the XRD data is also acknowledged with gratitude.

*Author to whom correspondence should be addressed. Email address: hearneg@physics.wits.ac.za

[1] M. Nicol and M. Y. Fong, J. Chem. Phys. **54**, 3167 (1971).
[2] G. A. Samara and P. S. Peercy, Phys. Rev. B **7**, 1131 (1973).
[3] Y. Hara and M. Nicol, Phys. Status Solidi B **94**, 317 (1979).
[4] T. Ohsaka, S. Yamaoka, and O. Shimomura, Solid State Commun. **30**, 345 (1979).
[5] J. F. Mammone, M. Nicol, and S. K. Sharma, J. Phys. Chem. Solids **42**, 379 (1981).
[6] H. Sato, S. Endo, M. Sugiyama, T. Kikegawa, O. Shimomura, and K. Kusaba, Science **251**, 786 (1991).
[7] J. Haines and J. M. Leger, Physica B **192**, 233 (1993).
[8] K. Lagarec and S. Desgreniers, Solid State Commun. **94**, 519 (1995).
[9] J. K. Dewhurst and J. E. Lowther, Phys. Rev. B **54**, R3673 (1996).
[10] T. Arlt, M. Beermejo, M. A. Blanco, L. Gerward, J. Z. Jiang, J. S. Olsen, and J. M. Recio, Phys. Rev. B **61**, 14414 (2000).
[11] L. S. Dubrovinsky, N. A. Dubrovinskaia, V. Swamy, J. Muscat, N. M. Harrison, R. Ahuja, *et al.*, Nature (London) **410**, 653 (2001).
[12] T. E. Mallouk, Nature (London) **353**, 698 (1991).
[13] X.-Z. Ding, X.-H. Liu, and Y.-Z. He, J. Mater. Sci. Lett. **15**, 1789 (1996).
[14] A. A. Gribb and J. F. Banfield, Am. Mineral. **82**, 717 (1997).
[15] Y. IIda, M. Furukawa, T. Aoki, and T. Sakai, Appl. Spectrosc. **52**, 673 (1998).
[16] R. L. Penn and J. F. Banfield, Am. Mineral. **84**, 871 (1999).
[17] H. Zhang and J. F. Banfield, J. Mater. Res. **15**, 437 (2000).
[18] W. F. Zhang, Y. L. He, M. S. Zhang, Z. Yin, and Q. Chen, J. Phys. D **33**, 912 (2000).
[19] J. S. Olsen, L. Gerward, and J. Z. Jiang, J. Phys. Chem. Solids **60**, 229 (1999); V. Swamy, L. S. Dubrovinsky, N. A. Dubrovinskaia, A. S. Simionovici, M. Drakopoulos, V. Dmitriev, and H. P. Weber, Solid State Commun. **125**, 111 (2003).
[20] Z. Wang, S. K. Saxena, V. Pischedda, H. P. Liermann, and C. S. Zha, J. Phys.: Condens. Matter **13**, 8317 (2001).
[21] Z. Wang and S. K. Saxena, Solid State Commun. **118**, 75 (2001).
[22] J. C. Parker and R. W. Siegel, Appl. Phys. Lett. **A66**, 943 (1990).
[23] Y. Machavariani, M. P. Pasternak, G. R. Hearne, and G. K. Rozenberg, Rev. Sci. Instrum. **69**, 1423 (1998).
[24] J. Zhao, G. Hearne, M. Maaza, M. K. Nieuwoudt, and J. D. Comins, Rev. Sci. Instrum. **71**, 4509 (2001).
[25] H. K. Mao, P. M. Bell, J. W. Shaner, and D. J. Steinberg, J. Appl. Phys. **49**, 3276 (1978).
[26] T. Ohsaka, F. Izumi, and Y. Fujiki, J. Raman Spectrosc. **7**, 321 (1978).
[27] J. C. Parker and R. W. Siegel, J. Mater. Res. **5**, 1246 (1990).
[28] J. S. Vermaak, C. W. Mays, and D. Kuhlmann-Wilsdorf, Surf. Sci. **12**, 128 (1968).
[29] D. Bersani, P. P. Lottici, and X.-Z. Ding, Appl. Phys. Lett. **72**, 73 (1998).
[30] M. Ivanda, S. Music, M. Gotic, A. Turkovic, A. M. Tonejc, and O. Gamulin, J. Mol. Struct. **480–481**, 641 (1999).
[31] D. A. Porter and K. E. Easterling, *Phase Transformations in Metals and Alloys* (Chapman & Hall, London, 1992).
[32] H. Zhang and J. F. Banfield, J. Mater. Chem. **8**, 2073 (1998).
[33] J. W. Cahn, Acta Metall. **28**, 1333 (1980).
[34] CCP14 website, http://www.ccp14.ac.uk/
[35] A. C. Larson and R. B. v. Dreele, Los Alamos National Laboratory, Report LAUR 86-748 (1994).
[36] C. J. Howard, T. M. Sabine, and F. Dickson, Acta Crystallogr., Sect. B: Struct. Sci. **B47**, 462 (1991).
[37] R. C. Cammamarata, Prog. Surf. Sci. **46**, 1 (1994).
[38] H. Ibach, Surf. Sci. Rep. **29**, 193 (1997).
[39] Consider a faceted nanoparticle with an equilibrium shape of a square plate with thickness $2x_1$ and width $2x_2$. If the surface stresses of the broad faces and edges are f_1 and f_2, respectively, then the excess pressure across the broad face is $\Delta P = 2f_2/x_2$, whereas the excess pressure across the edge is $\Delta P = f_1/x_1 + f_2/x_2$. These expressions are similar to the case of a spherical particle, and are derived by considering forces in equilibrium at each of the faces. The force exerted by the exposed perimeter of the broad face $4(2x_2)f_2$ must balance the force due to the excess pressure on that face $\Delta P\ (4x_2{}^2)$, and similarly for the edge faces of the faceted particle.
[40] P. S. Peercy and B. Morosin, Phys. Rev. B **7**, 2779 (1973).
[41] B. Kolk, *Studies of Dynamical Properties of Solids with the Mossbauer Effect* (Elsevier, Amsterdam, 1984).
[42] A. A. Maradudin and A. E. Fein, Phys. Rev. **128**, 2589 (1962).
[43] M. Horn, C. F. Schwerdtfeger, and E. P. Meagher, Z. Kristallogr. **136**, 273 (1972).
[44] J. Z. Jiang, J. S. Olsen, L. Gerward, and S. Morup, Europhys. Lett. **44**, 620 (1998).